Endogenous $GABA_A$ and $GABA_B$ receptor-mediated electrical suppression is critical to neuronal anoxia tolerance

Matthew E. Pamenter[a], David W. Hogg[b], Jake Ormond[c], Damian S. Shin[d], Melanie A. Woodin[b], and Leslie T. Buck[b,1]

[a]Department of Pediatrics, University of California at San Diego, La Jolla, CA 92037; [b]Department of Cell and Systems Biology and Ecology and Evolutionary Biology, University of Toronto, Toronto, ON, Canada M5S 3G5; [c]Canadian Centre for Behavioral Neuroscience, University of Lethbridge, Lethbridge, AB, Canada T1K 3M4; and [d]Center for Neuropharmacology and Neuroscience, Albany Medical College, Albany, NY 12208

Edited* by Mu-ming Poo, University of California, Berkeley, CA, and approved May 27, 2011 (received for review February 15, 2011)

Anoxic insults cause hyperexcitability and cell death in mammalian neurons. Conversely, in anoxia-tolerant turtle brain, spontaneous electrical activity is suppressed by anoxia (i.e., spike arrest; SA) and cell death does not occur. The mechanism(s) of SA is unknown but likely involves GABAergic synaptic transmission, because GABA concentration increases dramatically in anoxic turtle brain. We investigated this possibility in turtle cortical neurons exposed to anoxia and/or $GABA_{A/B}$ receptor (GABAR) modulators. Anoxia increased endogenous slow phasic GABAergic activity, and both anoxia and GABA reversibly induced SA by increasing $GABA_AR$-mediated postsynaptic activity and Cl^- conductance, which eliminated the Cl^- driving force by depolarizing membrane potential (~8 mV) to GABA receptor reversal potential (~−81 mV), and dampened excitatory potentials via shunting inhibition. In addition, both anoxia and GABA decreased excitatory postsynaptic activity, likely via $GABA_BR$-mediated inhibition of presynaptic glutamate release. In combination, these mechanisms increased the stimulation required to elicit an action potential >20-fold, and excitatory activity decreased >70% despite membrane potential depolarization. In contrast, anoxic neurons cotreated with $GABA_{A+B}R$ antagonists underwent seizure-like events, deleterious Ca^{2+} influx, and cell death, a phenotype consistent with excitotoxic cell death in anoxic mammalian brain. We conclude that increased endogenous GABA release during anoxia mediates SA by activating an inhibitory postsynaptic shunt and inhibiting presynaptic glutamate release. This represents a natural adaptive mechanism in which to explore strategies to protect mammalian brain from low-oxygen insults.

western painted turtle | cerebral cortex | channel arrest | pyramidal neurons | natural anesthetic mechanism

When deprived of oxygen, mammalian neurons are unable to produce sufficient ATP to meet cellular demands (1, 2). As a result, the Na^+/K^+ ATPase (Na^+ pump) fails and neuronal membrane potential (V_m) becomes unsustainable and anoxic depolarization (AD) follows, causing electrical hyperexcitability, deleterious Ca^{2+} influx, and spreading depression in the penumbral region (2, 3). Numerous studies have focused on the role of glutamatergic *N*-methyl-D-aspartate receptors (NMDARs) in this mechanism, and although NMDAR blockade prevents glutamatergic excitotoxicity (4), it does not prevent AD-mediated injury or postinsult apoptotic cell death (5). Thus, it is not surprising that clinical interventions targeting glutamate receptors alone have been largely ineffective against anoxic or ischemic damage (6), and therefore examination of alternative mechanisms to limit excitability during such insults is necessary.

A potential therapeutic alternative to directly antagonizing excitatory pathways is to up-regulate inhibitory mechanisms such as those mediated by γ-aminobutyric acid (GABA), the primary inhibitory neurotransmitter in the mature mammalian CNS (7). GABAergic mechanisms are not strongly recruited in ischemic mammalian neurons. In fact, although [GABA] is elevated by ~30% in ischemic murine brain, $GABA_A$ receptor subunit mRNA expression is decreased by ~85%, and GABA-evoked currents and [ATP] run down rapidly, suggesting endogenous GABAergic neuroprotection is transient and largely ineffective (8–10). Nonetheless, activating GABA receptors (GABARs) preinsult limits neuronal hyperexcitability in mammalian models of ischemic damage, and AD and cell death are not observed in the afflicted brain region (11, 12). Despite these promising results, GABA has received little attention as a clinical stroke intervention and the mode of GABAergic neuroprotection is poorly understood (13).

Unlike the modest increase observed in anoxic mammals, brain [GABA] is rapidly elevated in anoxia-tolerant species including freshwater turtles (*Chrysemys picta bellii*, *Trachemys scripta elegans*) and fish (*Carassius carassius*, *Carassius auratus*) (1, 14). These organisms achieve a large-scale reduction in cellular energy turnover and survive weeks to months of anoxic exposure without apparent detriment (1). The key to this tolerance may be an adaptive mechanism that combines depressed glutamatergic signaling with enhanced GABAergic signaling. Indeed, we have previously demonstrated that excitatory glutamatergic signaling (via NMDARs and α-amino-3-hydroxy-5-methyl-4-isoxazolepropionic acid receptors; AMPARs) is downregulated in these species during anoxia (15–17); however, the role of GABAergic signaling in anoxia tolerance has not been elucidated. In turtle brain, [GABA] is increased a remarkable 80-fold during anoxia and electrical activity is suppressed 75–95% (14, 18–20). Therefore, this organism provides a good model in which to examine the role of GABA in regulating electrical activity during anoxia. We hypothesized that increased GABAergic conductance to Cl^- mediates electrical suppression (i.e., spike arrest; SA) in the anoxic turtle cortex, and that in combination with glutamatergic channel arrest prevents hyperexcitability and provides neuroprotection against anoxic insults.

Results

Spike Arrest Is Comediated by $GABA_A$ and $GABA_B$ Receptors. We examined SA in pyramidal neurons from intact cortical sheets because synaptic connectivity and endogenous neurotransmitter release are maintained in this preparation ex vivo (18, 20, 21). In normoxia, stepwise current injections elicited action potentials (APs) at a threshold (AP_{th}) of −49.1 ± 2.0 mV and spontaneous APs occurred with a frequency (AP_f) of 2.1 ± 0.3 Hz (n = 15),

Author contributions: M.E.P., D.W.H., D.S.S., and L.T.B. designed research; M.E.P., D.W.H., J.O., and D.S.S. performed research; M.E.P., D.W.H., J.O., D.S.S., and M.A.W. analyzed data; and M.E.P. and L.T.B. wrote the paper.

The authors declare no conflict of interest.

*This Direct Submission article had a prearranged editor.

[1]To whom correspondence should be addressed. E-mail: les.buck@utoronto.ca.

This article contains supporting information online at www.pnas.org/lookup/suppl/doi:10.1073/pnas.1102429108/-/DCSupplemental.

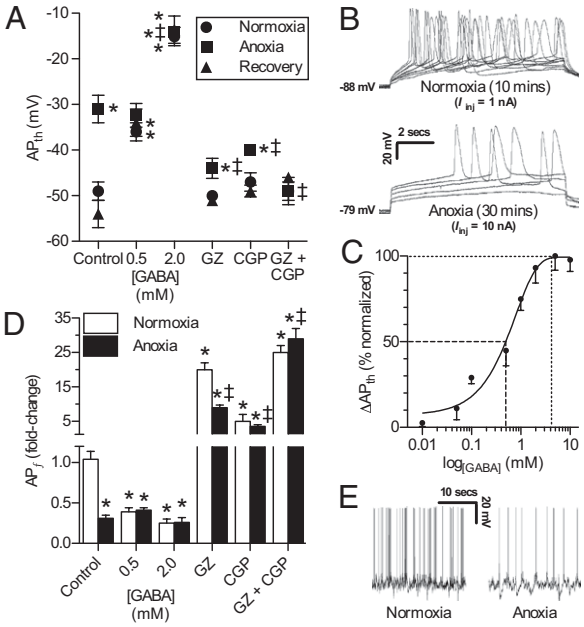

Fig. 1. Spike arrest in the anoxic turtle cortex is $GABA_{A+B}R$-mediated. (*A*) Summary of neuronal AP threshold (AP_{th}) during a normoxic-to-anoxic transition with recovery (t = 10, 30, and 60 min). (*B*) Sample recordings of APs stimulated from electrically quiet neurons by stepwise current injection. (*C*) Dose–response relationship of [GABA] versus ΔAP_{th}. (*D*) Summary of AP_f expressed as fold change relative to pretreatment baseline. (*E*) Sample V_m recordings of APs from *D*. Treatments: GABA, 25 μM gabazine ($GABA_AR$ antagonist), 5 μM CGP55845 ($GABA_BR$ antagonist). Data are mean ± SEM from 9–19 separate experiments. Asterisks indicate significant difference from normoxic controls. Double daggers indicate significant difference from anoxic controls ($P < 0.05$).

whereas during anoxia, AP_{th} depolarized to −31.1 ± 2.9 mV and AP_f decreased >70% (n = 19; Fig. 1 *A*, *B*, *D*, and *E*). These changes were reversed by reoxygenation and are consistent with previous reports of SA in anoxic turtle brain (15, 18, 20). GABA perfusion reversibly mimicked SA and depolarized AP_{th} in a dose-dependent fashion (n = 3–13 for each [GABA]; Fig. 1*C*), and at moderate (0.5 mM) or high (2.0 mM) [GABA], AP_{th} depolarized 20–35 mV and AP_f decreased 60–70% (n = 10–13 each; Fig. 1 *A* and *D*). Conversely, antagonism of $GABA_ARs$ (with 25 μM gabazine; GZ) or $GABA_BRs$ (with 5 μM CGP55845; CGP) each partially reduced the depolarization of AP_{th} and increased AP_f, whereas coantagonism of $GABA_{A+B}Rs$ abolished the anoxic depolarization of AP_{th} and increased AP_f 30- and 100-fold relative to normoxic and anoxic controls, respectively (n = 9–13 each; Fig. 1 *A* and *D*).

Endogenous GABA Release Increases During Anoxia and "Resets" V_m to GABA Receptor Reversal Potential. To directly assay anoxic changes in GABA release, we adapted techniques used elsewhere to examine GABAergic postsynaptic currents (PSCs) (9, 22), and used $GABA_ARs$ to detect anoxic changes in extracellular [GABA] (n = 8; Fig. 2*A*) (for these experiments only, currents were isolated and enhanced as described in *SI Materials and Methods* and Fig. 2). Under these conditions, a significant tonic inhibitory current was not observed (normoxic I_{tonic} = 1.6 ± 3.9 pA vs. anoxic I_{tonic} = 3.1 ± 2.4 pA; n = 8; Fig. 2*Aii*); however, spontaneous GABAergic slow phasic PSCs were detectable during normoxia, and their amplitude doubled during anoxic perfusion (41.2 ± 1.6 to 82.1 ± 2.1 pA; n = 10; Fig. 2 *Ai*, *B*, and *C*), whereas PSC_f was unchanged (Fig. S1*A*). PSCs were abolished by $GABA_AR$ antagonists (GZ or picrotoxin; PTX) and enhanced by GABA transporter antagonists (GAT; n = 4 each),

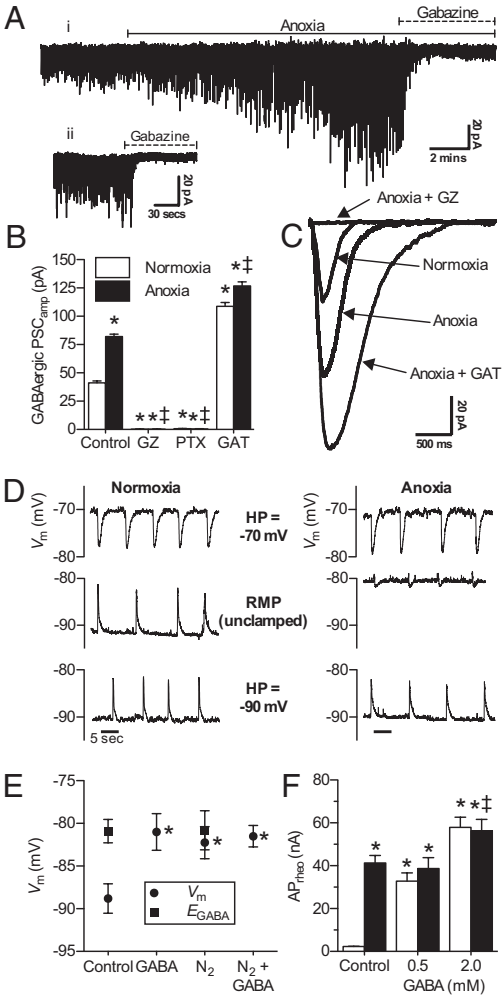

Fig. 2. Endogenous synaptic GABAergic activity is enhanced during anoxia and V_m resets to E_{GABA}. (*A*) (*i*) Raw spontaneous GABAergic current activity. (*ii*) Raw tonic GABAergic activity. To aide current detection, pipette [Cl^-] was increased to 110 mM and neurons were clamped at −100 mV and cotreated with the NMDAR antagonist APV (25 μM) and the AMPAR antagonist CNQX (25 μM). (*B*) Summary of GABAergic PSC_{amp}. Neurons were examined per *A*. (*C*) Superimposed raw spontaneous GABAergic PSC recordings averaged from 30 events from three neurons per trace. (*D*) Sample recordings of GABAergic PSPs in normoxia and anoxia from neurons voltage-clamped at −70 mV or −90 mV (top and bottom traces, respectively) or free-running (no voltage-clamp; middle traces) in the presence of APV and CNQX. RMP, resting membrane potential [holding potential (HP)]. (*E*) Summary of paired V_m and E_{GABA} measured in the perforated-patch configuration. APs were prevented by the voltage-gated Na^+ channel antagonist TTX (5 μM). (*F*) Summary of AP_{rheo} (I_{inj} to elicit an AP). Treatments were as in Fig. 1, with GABA transport inhibitors SKF 89976A hydrochloride (40 μM; GAT-1) and (S)-SNAP-5114 (20 μM; GAT-2 and -3). Data are mean ± SEM from 4–19 separate experiments. Asterisks indicate significant difference from normoxic controls. Double daggers indicate significant difference from anoxic controls ($P < 0.05$).

confirming postsynaptic $GABA_ARs$ activation by endogenous synaptic GABA release. To better understand this relationship, we measured native GABAergic postsynaptic potentials (PSPs) using the perforated-patch method to avoid perturbing intracellular [Cl^-] and in the presence of 6-cyano-7-nitroquinoxaline-2,3-dione (CNQX) and (2*R*)-amino-5-phosphonovaleric acid (APV) to isolate GABAergic events. Normoxic GABAergic PSP amplitude was 10.3 ± 1.8 mV, and events were depolarizing relative to V_m (n = 7; Fig. 2*D* and Fig. S1*B*). Similar to PSCs, GABAergic PSPs were abolished by GZ but not by CGP, indicating mediation by postsynaptic $GABA_ARs$ (n = 10–13 each).

NEUROSCIENCE

PSPs occurred at a rate of 0.1 ± 0.01 Hz, and this frequency was unchanged during anoxia (0.09 ± 0.02 Hz); however, anoxic PSPs were markedly smaller in amplitude (−1.47 ± 0.7 pA), and their polarity was reversed such that PSPs generally became mildly hyperpolarizing relative to V_m, indicating that the relationship between V_m and the reversal potential of Cl^- (E_{Cl}) is reset during anoxia. Importantly, when we current-clamped neurons at −90 mV (near normoxic V_m) or −70 mV (depolarized relative to both normoxic and anoxic V_m), the resulting PSPs were not different between conditions, indicating that the mechanism underlying this change is an alteration of V_m homeostasis during anoxia.

$GABA_AR$ activation induces Cl^- flux in the direction of E_{Cl} ($GABA_AR$ reversal potential; E_{GABA}) (7), which has not been previously measured in adult turtle brain. Therefore, to more closely examine the relationship between V_m and $GABA_AR$ activity, we examined E_{GABA}. In normoxic whole-cell experiments, E_{GABA} was −80.9 ± 1.4 mV, and ∼8 mV depolarized relative to V_m in the same neurons (−88.8 ± 1.7 mV; n = 10; Fig. 2*E*). E_{GABA} was unchanged during anoxic perfusion (−80.8 ± 2.3 mV; n = 8; Fig. 2*E* and Fig. S1*C*); however, V_m depolarized to −80.2 ± 1.9 mV. Consistent with an underlying GABAergic mechanism, normoxic GABA perfusion depolarized V_m in a dose-dependent fashion (n = 3–13 each [GABA]; Fig. S1*D*), and 2 mM GABA depolarized V_m to E_{GABA} in normoxia and anoxia (−81.0 ± 2.1, n = 12, and −81.5 ± 1.2 mV, n = 7, respectively). In separate experiments, we examined the effect of normoxic GABAR modulation on V_m and E_{GABA} in the perforated-patch configuration. Consistent with our whole-cell results, E_{GABA} was depolarized relative to V_m (−85.6 ± 0.8 and −91.8 ± 0.7 mV, respectively; n = 7; Fig. S1*E*), whereas during GABA perfusion, V_m depolarized to −84.3 ± 1.3 mV (n = 10) in a $GABA_AR$-dependent fashion (n = 7). [Note: E_{GABA} could not be determined during GABA or GZ perfusion due to $GABA_AR$ saturation or antagonism, respectively (Fig. 2*E* and Fig. S1 *E* and *F*).]

When E_{GABA} is depolarized relative to V_m, such as in the early stages of mammalian development and to a lesser degree in the anoxic turtle cortex, the Cl^- gradient is such that postsynaptic $GABA_AR$ activation induces Cl^- efflux accompanied by reductions in cell volume (7). Therefore, to confirm the relationships between V_m and E_{GABA} observed in our electrophysiology experiments, we examined Cl^- movement and neuronal volume regulation using noninvasive assays [6-methoxy-*N*-ethylquinolinium iodide (MEQ) and calcein-AM fluorescence, respectively] (23, 24). Anoxia or GABA perfusion reversibly increased MEQ fluorescence 30–40% in a $GABA_AR$-dependent fashion, reflecting Cl^- efflux, because intracellular Cl^- quenches MEQ fluorescence (n = 5 each; Fig. S1 *G* and *H*). Similarly, calcein fluorescence increased 22.1 ± 4.0 and 9.0 ± 3.0% during anoxia or GABA perfusion, respectively, reflecting cell shrinkage, whereas $GABA_{A+B}R$ antagonism reduced the anoxic increase by ∼80%, to 5.0 ± 7.7% (n = 4 each; Fig. S1 *I–K*). Therefore, unlike in most adult mammalian neurons, E_{GABA} is depolarized relative to normoxic V_m in adult turtle cortex. Furthermore, the $GABA_AR$-mediated increase in Cl^- conductance (G_{Cl}) is sufficiently large that E_{Cl} (E_{GABA}) becomes the primary determinant of V_m during anoxia, and V_m resets to E_{GABA}. Despite this initial mild depolarization of V_m, this mechanism strongly resisted further V_m depolarization beyond E_{GABA} because rheobase (AP_{rheo}; i.e., stimulation required to generate an AP) increased >15-fold during anoxia or GABA perfusion (n = 10–17 each; Fig. 2*F*).

$GABA_A$ and $GABA_BRs$ Mediate Distinct Post- and Presynaptic Mechanisms of SA. Because anoxia or GABA perfusion induced Cl^- efflux and V_m depolarization, we hypothesized that GABAR activation increased neuronal conductance to Cl^-. Not surprisingly, we found that anoxic perfusion reversibly increased neuronal whole-cell conductance (G_w) from 4.8 ± 0.3 to 6.7 ± 0.4 nS (n = 17 for each; Fig. 3 *A* and *B*) (see comment on previous G_w measurements in anoxic turtle neurons in *SI Materials and Methods*). This change was abolished by GZ but not by CGP (n = 7 each), whereas GABA perfusion increased G_w in a dose-dependent fashion (n = 3–13 for each [GABA]; Fig. 3*C*). Importantly, pretreatment with 0.5 mM GABA raised baseline G_w to 8.1 ± 0.6 nS (n = 9; Fig. 3*A*); however, following the transition to anoxia, G_w decreased to 6.6 ± 0.4 nS and this change was prevented by GZ (n = 9 each). This suggests the magnitude of the anoxic change in G_{Cl} was partially masked in our experiments, because G_w is a global cellular measurement that includes the conductance of all open channels and receptors. This is particularly relevant in this model because previous studies have demonstrated channel arrest of AMPARs (G_{Na}) and NMDARs ($G_{Na/Ca}$), decreased K^+ leakage, and reduced K^+ and Na^+ channel and NMDAR density in anoxic turtle brain (1, 15), all of which would mask the $GABA_AR$-mediated G_{Cl}. To isolate ΔG_{Cl} from these confounding anoxic changes, we examined the effects of GABA on normoxic input resistance (R_{in}; the inverse of G_w) using the gramicidin perforated-patch technique. In support of our hypothesis that ΔG_{Cl} was partially obscured during anoxia, GABA reversibly decreased R_{in} ∼85%, from 314.5 ± 50.2 to 72.1 ± 13 MΩ (n = 10 and 7, respectively; Fig. S2 *A* and *B*), and this change was prevented by GZ but not by CGP (n = 8 and 6, respectively). Therefore, increased GABA release enhanced $GABA_AR$-mediated PSP activity and activated a large G_{Cl}, which was the primary determinant of G_w homeostasis during anoxia, causing V_m to depolarize to E_{GABA}.

CGP perfusion increased action potential frequency approximately fivefold in both normoxia and anoxia (Fig. 1*D*) but, unlike

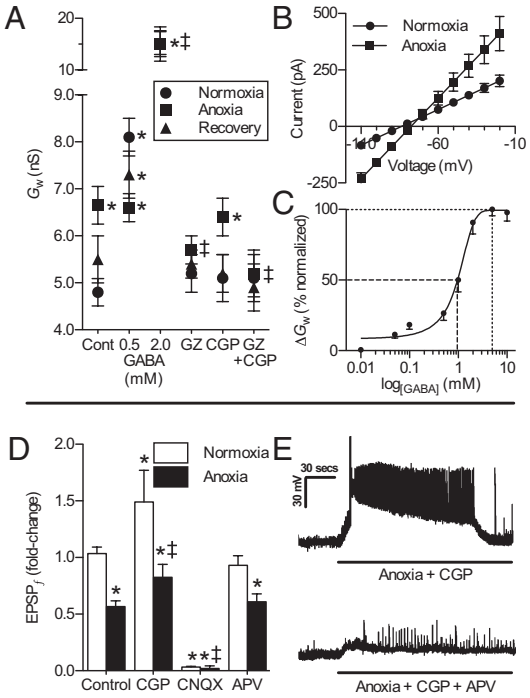

Fig. 3. $GABA_AR$ activation induces a shunt-like increase in plasma membrane permeability to Cl^-; $GABA_BR$ activation decreases EPSP activity via a presynaptic mechanism. (*A*) Summary of G_w measured in the whole-cell configuration. (*B*) *I–V* relationships from *A*. (*C*) Dose–response relationship of [GABA] versus G_w. (*D*) Summary of $EPSP_f$ expressed as fold change relative to pretreatment baseline. (*E*) Sample V_m recordings from neurons treated as indicated. Black bars represent duration of treatment. Treatments were as in Figs. 1 and 2. Data are mean ± SEM from 6–19 separate experiments. Asterisks indicate significant difference from normoxic controls. Double daggers indicate significant difference from anoxic controls (P < 0.05).

GZ, had no effect on G_w (Fig. 3*A*). This suggests that $GABA_B$R-mediated inhibition occurs at the presynapse. Excitatory postsynaptic potentials (EPSPs) are mediated by presynaptic glutamate release, and unlike the dramatic increase characteristic of ischemic mammalian brain, [glutamate] decreases 47% in anoxic turtle brain due to a combination of sustained reuptake and reduced release, and glutamatergic $EPSP_f$ and amplitude decrease (1, 2, 15). Glutamate release can be inhibited by agonism of presynaptic $GABA_B$Rs, which activate K^+ channels that hyperpolarize presynaptic cells and also inhibit Ca^{2+} channels that mediate vesicular glutamate release (25). Because [GABA] is elevated in anoxic turtle brain (14), such presynaptic mechanisms likely contribute to SA by decreasing postsynaptic glutamatergic drive. In support of this, we found that CGP enhanced AMPAergic $EPSP_f$ in both normoxia and anoxia (n = 9–13 each; Fig. 3*D*). Furthermore, antagonizing NMDARs with APV prevented hyperexcitability in anoxic CGP-challenged neurons, and APs were prevented despite the CGP-mediated enhancement of EPSP activity during anoxia (n = 5; Fig. 3*E*).

GABAergic SA Is Critical to Anoxia Tolerance in Turtle Neurons. To assess the importance of GABAergic mechanisms in anoxia tolerance, we measured hallmarks of excitotoxic cell death (ECD) characteristic of ischemic mammalian neurons, including hyperexcitability, AD, deleterious Ca^{2+} influx, and cell death (2, 3). Similar to previous examinations in turtle cortex, these parameters were unchanged in normoxia, whereas during anoxia, V_m depolarized to E_{GABA} (n = 12) and cytosolic calcium concentration ($[Ca^{2+}]_c$) increased ~30% (n = 5; Fig. 4 *A* and *B* and Fig. S3 *A* and *B*) (1, 17, 26). Anoxic changes were reversed by reperfusion, indicating turtle neurons were not significantly stressed. Similarly, propidium iodide (PI) uptake [assessed relative to maximum uptake in metabolically arrested neurons treated with iodoacetate (IAA) and sodium cyanide (NaCN); Fig. S3 *D* and *E*] was unchanged during 4 h of normoxia or anoxia (n = 3 each; Fig. 4 *A* and *B* and Fig. S3*C*).

In striking contrast, neurons cotreated with GZ and CGP underwent recurrent seizure-like events (SLEs) and terminal depolarization of V_m (n = 17), a fourfold increase in $[Ca^{2+}]_c$ during anoxia that became further elevated to >1 μM during reperfusion (n = 4), and an increase in PI uptake within 2 h of treatment onset that at 4 h was elevated four- and sevenfold above normoxic and anoxic controls (n = 3; Fig. 4*C* and Fig. S3 *A*–*C*). This suggests SA is critical to anoxia tolerance because blocking the inhibitory GABAergic activity sensitized V_m to depolarizing inputs, resulting in unsustainable electrical hyperexcitation and terminal depolarization of V_m. We hypothesized that SA is predominately mediated by a $GABA_A$R-dependent electrical shunt mechanism that is passively recruited to oppose spontaneous excitatory events. If correct, pharmacological inhibition of APs with voltage-gated Na^+-channel antagonist tetrodotoxin (TTX) should limit electrical excitability in $GABA_{A+B}$R-antagonized neurons, eliminate the requirement of SA as critical for anoxia tolerance, and ameliorate cytotoxicity despite persistent $GABA_A$R blockade and enhanced presynaptic glutamate release. In support of this, TTX inhibited APs and prevented SLEs (n = 6), deleterious $[Ca^{2+}]_c$ accumulation (n = 4), and PI uptake by $GABA_{A+B}$R-antagonized anoxic neurons (n = 4; Fig. 4*D* and Fig. S3 *A*–*C*).

Discussion

Using a naturally anoxia-tolerant model, we show that $GABA_{A/B}$Rs are critical to SA and neuronal survival against low-oxygen insult in an anoxia-tolerant species. Importantly, we also show through the use of GABA uptake blockers and $GABA_{A/B}$R antagonists that the anoxic response is sensitive to endogenous synaptic GABA release and activates distinct inhibitory mechanisms on pre- and postsynaptic cells. The primary mechanism of SA is an increase in slow phasic $GABA_A$R-mediated PSP activity, which opens a postsynaptic G_{Cl} that dominates G_w during anoxia. We propose that this conductance acts as an inhibitory electrical shunt that effectively clamps V_m at E_{GABA} during anoxia, opposing further V_m depolarization due to glutamatergic EPSPs. This is likely the primary mechanism underlying anoxic SA, because $GABA_A$R antagonism is significantly more excitatory than $GABA_B$R antagonism. Nonetheless, $GABA_B$R activation contributes to SA by decreasing postsynaptic $EPSP_f$ during anoxia, presumably via inhibition of presynaptic glutamate release. Importantly, V_m depolarization, such as the shift to E_{GABA} we report here, is usually excitatory in neurons (7); however, the voltage separation between V_m and AP_{th} paradoxically increases during anoxia because AP_{th} depolarizes twofold further than V_m. Therefore, although anoxic neurons depolarize to E_{GABA}, V_m is hyperpolarized relative to AP_{th}, and the net effect of these changes is inhibitory. Indeed, despite V_m depolarization, rheobase increases ~20-fold during anoxia and fewer APs are elicited by each supra-AP_{th} stimulus train.

E_{GABA} is primarily determined by the Cl^- gradient, which is in turn dependent upon the balance in expression and activity of Na^+-K^+-Cl^- (NKCC1) (Cl^- influx) and K^+-Cl^- (KCC2) (Cl^- efflux) cotransporters (7). In developing mammalian brain, KCC2 expression is low relative to NKCC1, and GABA is the

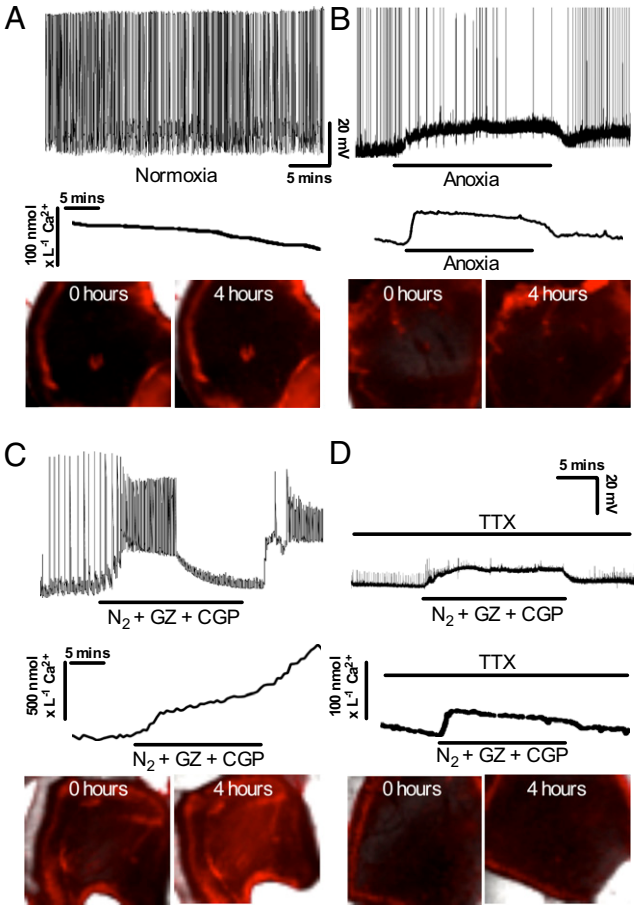

Fig. 4. Pharmacological inhibition of endogenous inhibitory GABAergic mechanisms during anoxia is excitotoxic to turtle neurons. Sample V_m recordings (upper trace in each grouping), fura-2 Ca^{2+} fluorescence recordings (lower trace), and paired raw PI fluorescence images before treatment onset (t = 0 h) and following 4 h of treatment from neurons treated with normoxia (*A*), anoxia (*B*), anoxia + $GABA_{A+B}$R antagonists (*C*), and anoxia + $GABA_{A+B}$R antagonists in the presence of TTX (*D*). Black bars represent duration of treatment. Treatments were as in Figs. 1 and 2.

NEUROSCIENCE

primary excitatory neurotransmitter. As a result, mammalian neonate brain is particularly prone to hyperexcitability and seizures, but can be protected by simultaneously inhibiting NKCC1 and antagonizing postsynaptic $GABA_A$Rs to temporarily switch the Cl^- gradient and render GABA inhibitory (27). Conversely, in adult mammalian brain, KCC2 expression is high and E_{GABA} is generally hyperpolarized relative to V_m (7). Therefore, GABA perfusion opposes AP generation by hyperpolarizing V_m away from AP_{th} via $GABA_A$R-mediated Cl^- influx; however, this form of inhibition requires increased Na^+-pump activity to maintain ion gradients and is therefore not an effective strategy (1).

In adult mammalian brain, endogenous synaptic GABA release in the first few minutes of ischemia slows the onset of AD; however, this limited inhibition is insufficient to preserve [ATP] and maintain ion pumping >2–3 min (9). As a result, ion gradients are lost and extracellular K^+ concentration ($[K^+]_o$) increases sharply, causing AD within ∼6 min of insult (2, 3, 9). Extracellular neurotransmitter levels also increase rapidly in the first few minutes of ischemia (2, 9, 22), and glutamatergic Na^+ and Ca^{2+} influx quickly depolarizes V_m away from E_{GABA}, thereby enhancing AD and also the inward-driving force on Cl^-. When extracellular GABA activates $GABA_A$Rs, large-scale Cl^- and associated water influx occurs (9, 23). This abrupt osmotic shift causes ischemic cells to swell and, depending on the severity of AD, undergo necrotic membrane rupture (28). This problem is compounded by impaired cerebral blood flow (CBF), which limits the removal of deleterious ions and neurotransmitters, the extracellular accumulation of which are required for ischemia-related cell swelling (2, 29). In contrast, CBF is maintained during prolonged anoxia in adult turtle brain (1), and synaptic transmission persists in vivo and in vitro (18, 19, 30; present report). Furthermore, $[K^+]_o$, and cellular [ATP] are maintained for at least 6 h in anoxic turtle brain (30), and cells do not exhibit a necrotic phenotype. Finally, whereas ischemic adult mammalian neurons swell, anoxic turtle neurons shrink because E_{GABA} is depolarized relative to normoxic V_m, and therefore anoxic activation of $GABA_A$Rs causes Cl^- and water efflux and thus cell-volume reduction. To our knowledge, the inhibitory depolarized relationship between E_{GABA} and V_m we report in adult turtle neurons is a unique phenotype and may represent an evolutionary adaptation that allows this species to retain neuronal function while reducing energy expenditure during prolonged anoxia.

This unique phenotype of GABAergic inhibition contributes crucial energy savings by reducing the demand on ATPases and related cotransporters during anoxia. The bulk of these savings is attributable to the GABA-mediated decrease in AP firing (i.e., SA), which reduces activity-induced perturbations of ionic gradients and the requirement for compensatory Na^+-pump activity (1). In addition, V_m resets to E_{GABA} during anoxia, and is depolarized relative to normoxia, which further reduces pump demand. Also, because GABAergic G_{Cl} dominates G_w during anoxia, the importance of G_K in determining V_m is reduced. As a result, K^+-channel expression and G_K are decreased without detriment in anoxic turtle brain, and the pump activity required to maintain K^+ gradients is inherently reduced (1, 30). Finally, glutamate reuptake is sustained during anoxia in turtle brain and is also primarily dependent on ATPase activity (31). $GABA_B$R-mediated inhibition of presynaptic glutamate release limits the workload on these pumps, further reducing ATP consumption. Indeed, turtle brain Na^+-pump activity is known to decrease ∼35% during anoxia (1); therefore, when combined, these effects provide significant energy savings and suppress neuronal excitability sufficiently to maintain [ATP] and V_m despite a >90% reduction in ATP production during anoxia (1). This conclusion is supported by the observations that: (*i*) $GABA_{A+B}$R inhibition prevents anoxia-mediated SA and neurons exhibit hallmarks of ECD, indicating that in the absence of GABAergic inhibition, anaerobic ATP production is insufficient to sustain V_m homeostasis; and (*ii*) simultaneous inhibition of $GABA_{A+B}$Rs and voltage-gated Na^+ channels prevented the $GABA_{A+B}$R antagonist-mediated increase in excitatory activity and ECD during anoxia.

The lack of a measurable tonic inhibitory current in turtle cortical neurons is an important finding. Tonic currents are mediated by extrasynaptic $GABA_A$Rs and set the excitability threshold for neurons in adult mammalian brain (32). Baseline tonic inhibition is typically >50 pA, and this activity increases greater than twofold postischemic insult in mammals and impairs functional recovery following stroke (9, 33). Conversely, anoxia-tolerant turtle cortical neurons likely do not express extrasynaptic $GABA_A$Rs because they lack an observable tonic current. This is not uncommon; many cell types do not express these receptors (32). More importantly, because E_{GABA} is depolarizing relative to V_m in normoxic turtle brain, any tonic GABAergic activity would be excitatory, and therefore the absence of such a tone in this model is not surprising. Indeed, the lack of any tonic inhibition minimizes the cellular signal-to-noise ratio of synaptic GABAergic inputs, and would therefore acutely sensitize turtle neurons to slow phasic (i.e., synaptic $GABA_A$R-mediated) inhibition.

The phenotype of phasic GABAergic inhibition in this model is unique: Slow phasic GABAergic activity occurs during normoxia at a frequency that is ∼1/15th that of resting mammalian neurons (9). This activity doubles in amplitude but is unchanged in frequency throughout >30 min of anoxic exposure, whereas phasic frequency in ischemic mammalian neurons increases 20-fold (and 300-fold relative to anoxic turtle neurons) within seconds of insult onset, and $GABA_A$Rs quickly become desensitized to extracellular GABA binding after ∼10 min due to NMDAR-mediated Ca^{2+} accumulation (9). In comparison, the phasic GABAergic response in anoxic turtle brain is sustained, likely because Ca^{2+}-mediated $GABA_A$R desensitization is prevented in turtle by concurrent glutamatergic channel arrest and maintenance of $[Ca^{2+}]_c$ homeostasis during prolonged anoxia (15, 17), and because the lack of an underlying tonic baseline allows for considerably greater inhibition from a relatively modest increase in phasic activity.

It is important to note that although GABAergic pathways are pivotal to the anoxia tolerance of turtle neurons, several other mechanisms act in concert to provide this neuroprotection. Indeed, in turtle cortical neurons in which channel arrest of NMDARs is prevented, excitotoxicity is also observed (34), suggesting multiple mechanisms may provide critical contributions to anoxia tolerance in parallel. Nonetheless, these mechanisms combine to reduce whole-animal energy consumption >90% during anoxia, which matches the decrease in energy produced anaerobically relative to aerobic (normoxic) respiration (for a review, see ref. 1) and allows these animals to tolerate long-term anoxic insults. Many of these mechanisms cannot easily be adapted to mammals; however, cell-level mechanisms such as glutamatergic channel arrest and GABAergic up-regulation are more readily mimicked in mammalian brain and would provide significant energy savings during low-oxygen stresses. Indeed, in normoxic rat brain, AP generation and propagation and EPSPs account for ∼81% of neuronal energy expenditure (35).

In conclusion, we report that SA of turtle cortical neurons is key to prolonged anoxia tolerance and is mediated by unique inhibitory GABAergic mechanisms that combine increased $GABA_{A+B}$R activity with a mildly depolarized E_{GABA} to reduce AP firing and ATP demand. Although this phenotype appears to be unique to the adult turtle CNS, the elucidation of these endogenous inhibitory systems provides insight into effective neuroprotective strategies against low-oxygen insult that may be adapted to protect hypoxia-sensitive mammalian brain against stroke. Mimicking the combined GABAergic and glutamatergic

phenotype of anoxic turtle brain by activating $GABA_{A+B}Rs$ while inhibiting KCC2 activity and AMPAR and NMDAR conductance may prove to be neuroprotective in mammalian stroke models, and this hypothesis deserves further evaluation. Finally, the turtle enters into a comatose state during prolonged anoxia and EEG activity is decreased to basal levels (19). Because general anesthetics are hypothesized to induce a comatose state through the inhibition of excitatory glutamatergic and enhancement of GABAergic neurotransmission (36), as we have shown in the anoxic turtle, it is tempting to speculate that this model represents a natural anesthetic mechanism.

Materials and Methods

This study was approved by the University of Toronto Animal Care Committee. Cortical slice dissection and anoxic whole-cell patch-clamp recording methods are described elsewhere (21, 26). Briefly, cortical sheets were dissected and placed in a bath with a flow-through perfusion system. Anoxia was achieved by gassing the perfusate with 95% N_2/5% CO_2. Perfusion lines were double-jacketed, the bath chamber was covered, and all air spaces were similarly gassed. Neurons were perfused with pharmacological modifiers and/or anoxia as specified in *Results*. Electrical activity was recorded for up to 2 h from pyramidal neurons. For perforated-patch experiments, electrodes were backfilled with a KCl solution containing 25 μg/mL gramicidin.

Methods for dye-loading and fluorescence experiments are described previously (17). Baseline fluorescence was recorded for 10–20 min and then the tissue was exposed to treatment for up to 80 min and then reperfused. Ca^{2+} changes were assessed using 5 μM fura-2. Cl^- changes were assessed using MEQ. Changes in MEQ fluorescence were calibrated using the Stern–Volmer equation as described elsewhere (23). Cell-volume changes were measured using calcein-AM (24). Cell death was assessed using a PI exclusion assay. PI fluorescence due to IAA plus NaCN treatment was assessed as maximal cell death, and each treatment group was normalized to this value.

Statistical Analysis. Normalized data were analyzed using two-way ANOVA with a Student–Newman–Keuls post hoc test to compare within and against treatment and normoxic values. Significance was determined at $P < 0.05$.

ACKNOWLEDGMENTS. A Natural Sciences and Engineering Research Council of Canada Discovery grant, a Discovery Accelerator award to L.T.B., and Ontario Graduate Scholarships in Science and Technology to M.E.P. and D.H. supported this work.

1. Bickler PE, Buck LT (2007) Hypoxia tolerance in reptiles, amphibians, and fishes: Life with variable oxygen availability. *Annu Rev Physiol* 69:145–170.
2. Hansen AJ (1985) Effect of anoxia on ion distribution in the brain. *Physiol Rev* 65: 101–148.
3. Leao AAP (1944) Spreading depression of activity in the cerebral cortex. *J Neurophysiol* 7:359–390.
4. Sattler R, Tymianski M (2000) Molecular mechanisms of calcium-dependent excitotoxicity. *J Mol Med* 78:3–13.
5. Buchan A, Pulsinelli WA (1990) Hypothermia but not the *N*-methyl-D-aspartate antagonist, MK-801, attenuates neuronal damage in gerbils subjected to transient global ischemia. *J Neurosci* 10:311–316.
6. Ikonomidou C, Turski L (2002) Why did NMDA receptor antagonists fail clinical trials for stroke and traumatic brain injury? *Lancet Neurol* 1:383–386.
7. Blaesse P, Airaksinen MS, Rivera C, Kaila K (2009) Cation-chloride cotransporters and neuronal function. *Neuron* 61:820–838.
8. Erecińska M, Nelson D, Wilson DF, Silver IA (1984) Neurotransmitter amino acids in the CNS. I. Regional changes in amino acid levels in rat brain during ischemia and reperfusion. *Brain Res* 304:9–22.
9. Allen NJ, Rossi DJ, Attwell D (2004) Sequential release of GABA by exocytosis and reversed uptake leads to neuronal swelling in simulated ischemia of hippocampal slices. *J Neurosci* 24:3837–3849.
10. Li H, Siegel RE, Schwartz RD (1993) Rapid decline of $GABA_A$ receptor subunit mRNA expression in hippocampus following transient cerebral ischemia in the gerbil. *Hippocampus* 3:527–537.
11. Galeffi F, Sinnar S, Schwartz-Bloom RD (2000) Diazepam promotes ATP recovery and prevents cytochrome *c* release in hippocampal slices after in vitro ischemia. *J Neurochem* 75:1242–1249.
12. Costa C, et al. (2004) Coactivation of GABA(A) and GABA(B) receptor results in neuroprotection during in vitro ischemia. *Stroke* 35:596–600.
13. Ginsberg MD (2008) Neuroprotection for ischemic stroke: Past, present and future. *Neuropharmacology* 55:363–389.
14. Nilsson GE, Lutz PL (1991) Release of inhibitory neurotransmitters in response to anoxia in turtle brain. *Am J Physiol* 261:R32–R37.
15. Pamenter ME, Shin DS, Buck LT (2008) AMPA receptors undergo channel arrest in the anoxic turtle cortex. *Am J Physiol Regul Integr Comp Physiol* 294:R606–R613.
16. Wilkie MP, et al. (2008) Evidence of anoxia-induced channel arrest in the brain of the goldfish (*Carassius auratus*). *Comp Biochem Physiol C Toxicol Pharmacol* 148:355–362.
17. Bickler PE, Donohoe PH, Buck LT (2000) Hypoxia-induced silencing of NMDA receptors in turtle neurons. *J Neurosci* 20:3522–3528.
18. Pérez-Pinzón MA, Chan CY, Rosenthal M, Sick TJ (1992) Membrane and synaptic activity during anoxia in the isolated turtle cerebellum. *Am J Physiol* 263:R1057–R1063.
19. Fernandes JA, et al. (1997) Electroencephalogram activity in the anoxic turtle brain. *Am J Physiol* 273:R911–R919.
20. Feng ZC, Rosenthal M, Sick TJ (1988) Suppression of evoked potentials with continued ion transport during anoxia in turtle brain. *Am J Physiol* 255:R478–R484.
21. Blanton MG, Lo Turco JJ, Kriegstein AR (1989) Whole cell recording from neurons in slices of reptilian and mammalian cerebral cortex. *J Neurosci Methods* 30:203–210.
22. Rossi DJ, Oshima T, Attwell D (2000) Glutamate release in severe brain ischaemia is mainly by reversed uptake. *Nature* 403:316–321.
23. Inglefield JR, Schwartz-Bloom RD (1999) Fluorescence imaging of changes in intracellular chloride in living brain slices. *Methods* 18:197–203.
24. Hamann S, et al. (2002) Measurement of cell volume changes by fluorescence self-quenching. *J Fluoresc* 12:139–145.
25. Bettler B, Kaupmann K, Mosbacher J, Gassmann M (2004) Molecular structure and physiological functions of GABA(B) receptors. *Physiol Rev* 84:835–867.
26. Pamenter ME, Buck LT (2008) Neuronal membrane potential is mildly depolarized in the anoxic turtle cortex. *Comp Biochem Physiol A Mol Integr Physiol* 150:410–414.
27. Dzhala VI, et al. (2005) NKCC1 transporter facilitates seizures in the developing brain. *Nat Med* 11:1205–1213.
28. Otsubo K, Katayama Y, Terashi A (1993) Protective effects of glycerol and mannitol on delayed neuronal death in the gerbil hippocampus (Translated from Japanese). *Nippon Ika Daigaku Zasshi* 60:231–240.
29. Yi CS, Fogelson AL, Keener JP, Peskin CS (2003) A mathematical study of volume shifts and ionic concentration changes during ischemia and hypoxia. *J Theor Biol* 220: 83–106.
30. Chih CP, Feng ZC, Rosenthal M, Lutz PL, Sick TJ (1989) Energy metabolism, ion homeostasis, and evoked potentials in anoxic turtle brain. *Am J Physiol* 257: R854–R860.
31. Milton SL, Thompson JW, Lutz PL (2002) Mechanisms for maintaining extracellular glutamate levels in the anoxic turtle striatum. *Am J Physiol Regul Integr Comp Physiol* 282:R1317–R1323.
32. Mody I, Glykys J, Wei W (2007) A new meaning for "gin & tonic": Tonic inhibition as the target for ethanol action in the brain. *Alcohol* 41:145–153.
33. Clarkson AN, Huang BS, Macisaac SE, Mody I, Carmichael ST (2010) Reducing excessive GABA-mediated tonic inhibition promotes functional recovery after stroke. *Nature* 468:305–309.
34. Pamenter ME, Buck LT (2008) δ-Opioid receptor antagonism induces NMDA receptor-dependent excitotoxicity in anoxic turtle cortex. *J Exp Biol* 211:3512–3517.
35. Attwell D, Laughlin SB (2001) An energy budget for signaling in the grey matter of the brain. *J Cereb Blood Flow Metab* 21:1133–1145.
36. Campagna JA, Miller KW, Forman SA (2003) Mechanisms of actions of inhaled anesthetics. *N Engl J Med* 348:2110–2124.

Supporting Information

Pamenter et al. 10.1073/pnas.1102429108

SI Materials and Methods

Animals. This study was approved by the University of Toronto Animal Care Committee and conforms to the relevant guidelines issued by the Canadian Council on Animal Care regarding the care and use of experimental animals. Adult turtles (carapace diameter >15 cm) weighing 300–600 g were obtained from Niles Biological. Turtles were housed as described previously (1). All experiments were conducted at room temperature (22 °C).

Whole-Cell Electrophysiology. Cortical slice dissection and anoxic whole-cell patch-clamp recording methods are described elsewhere (2, 3). Briefly, whole cortical sheets were perfused with artificial cerebral spinal fluid [ACSF; 107 mM NaCl, 2.6 mM KCl, 1.2 mM $CaCl_2$, 1 mM $MgCl_2$, 2 mM NaH_2PO_4, 26.5 mM $NaHCO_3$, 10 mM glucose, 5 mM imidazole (pH 7.4); osmolarity 280–290 mOsmol/L], and whole-cell recordings were performed using the voltage-clamp method with 5- to 8-MΩ electrodes containing the following: 8 mM NaCl, 0.0001 mM $CaCl_2$, 10 mM NaHepes, 130 mM Kgluconate, 1 mM $MgCl_2$, 0.3 mM NaGTP, 2 mM NaATP (adjusted to pH 7.4). Typical whole-cell access resistance (R_a) was 10–30 MΩ. R_a was determined before each measurement of electrical activity (see below) and patches were discarded if R_a changed by more than 20% during the course of an experiment. The liquid junction potential was assessed as ∼7 mV, and all data have been corrected for this value offline (raw data traces are unaltered) (4). Spontaneous electrical activity was recorded for up to 2 h from pyramidal neurons identified as described elsewhere (1), and patches onto other types of cells were discarded. Action potentials (APs) and postsynaptic potentials (PSPs) were assessed using waveform template analysis in Clampfit 10 software (Axon Instruments). AP threshold (AP_{th}) was determined by injecting current in a ramp manner in 1- or 10-nA steps until an AP was elicited. Endogenous GABA release was examined by measuring tonic and phasic currents. Tonic activity was determined by subtracting the baseline current after 5 min gabazine (GZ) application from the pre-GZ baseline current, and phasic activity was determined by measuring the last 10–15 spontaneous postsynaptic current (PSC) events recorded under each treatment condition. To enhance tonic and phasic GABAergic current detection, neurons were clamped at a holding potential of −100 mV and pipette [Cl^-] was increased to 110 mM by equimolar substitution of KCl for Kgluconate. Recordings were performed in the presence of 6-cyano-7-nitroquinoxaline-2,3-dione (CNQX) and (2*R*)-amino-5-phosphonovaleric acid (APV) (25 μM each) to isolate GABA currents. To determine whether PSCs were elicited by endogenous GABA release, currents were blocked by GABAR antagonists and enhanced by the GABA transport (GAT) inhibitors SKF 89976A hydrochloride (GAT-1) and (S)-SNAP-5114 (GAT-2 and -3). Whole-cell conductance (G_w) was assessed by clamping neurons at voltage steps from −60 to −90 mV in 3-mV increments lasting 250 ms. Current values were measured between 200 and 220 ms to avoid any capacitance effects, and a slope conductance (or G_w) was determined from the resultant current–voltage relationship (5).

The whole-cell electrophysiology technique has previously been used to determine E_{GABA} in neurons (6, 7). The reversal potential of the GABA-induced current (E_{GABA}) was measured using 2-s ramp voltage steps from −110 to −20 mV applied before and after GABA application in the presence of 2 μM tetrodotoxin (TTX) to inhibit APs at depolarized potentials. *I–V* relationships were analyzed by taking the linear regression of each line before and after 2 mM GABA application, and E_{GABA} was estimated by measuring the voltage at which the *I–V* relationships before and during GABA application intersected, as described elsewhere (8). This intersection point is the voltage at which there is no difference in current between the normoxic (or anoxic) and GABA treatments and is a measure of the cell's background current indicating no effect of GABA perfusion and therefore the GABA reversal potential.

Perforated-Patch Electrophysiology. We used the gramicidin perforated-patch technique to examine neuronal electrical properties and to determine E_{GABA} without perturbing neuronal Cl^- gradients. For perforated-patch experiments, WPI TW150F-3 thin-walled 4- to 5-MΩ borosilicate glass electrodes were pulled and backfilled with a high-[Cl^-] solution (150 mM KCl) containing 25 μg/mL gramicidin. In this configuration, patches with R_a <50 MΩ were used for experiments. Slices were visualized using an Olympus BX51W1 microscope with infrared differential interference contrast optics and stimulated at 0.1 Hz for 100-μs duration with an A.M.P.I. isoflex stimulator triggered by an A.M.P.I. master8-stimulating electrode. Data were recorded using an Axon multiclamp 700B amplifier and analyzed with Clampex 9 software (Axon Instruments).

Previous Measurements of G_w in Turtle Cortex. There is disagreement in the literature regarding the effect of anoxia on G_w [the inverse of input resistance (R_{in})] in the anoxic turtle cortex, with one laboratory reporting an increase in G_w (9) and our laboratory reporting a decrease (5). In previous experiments from our laboratory, G_w was measured in neurons patched with electrodes containing 30 mM [Cl^-]; however, in our present experiments, we use a more physiologically relevant 10 mM [Cl^-] in whole-cell experiments and also perforated-patch analysis, and report an increase in G_w with anoxia that agrees with the previously reported decrease in R_{in} (9). We used the Nernst equation and our perforated-patch measurements of E_{GABA} and determined that physiological $[Cl^-]_c$ is <10 mM in these neurons.

Live-Cell Fluorescence Imaging. Methods for cortical sheet isolation, dye loading, and anoxic fluorescence experiments are described previously (10). Baseline fluorescence was recorded for 10–20 min until the signal was stable and then the tissue was exposed to treatment ACSF for up to 80 min. Tissues were then reperfused with control ACSF. For each experiment, 50 neurons were chosen at random and the average change of fluorescence in the cell body of these neurons was used for statistical comparison. Brightly fluorescing cells were avoided. Data were analyzed using EasyRatioPro software (Photon Technology International). For all dyes, changes in background fluorescence in cortical sheets exposed to each treatment were assessed in the absence of fluorophores. None of the treatments resulted in changes in background fluorescence for the dyes examined.

Calcium changes were assessed using 5 μM fura-2 excited at 340 and 380 nm. Cytosolic calcium concentration ($[Ca^{2+}]_c$) was calculated as described elsewhere (11). Chloride changes were assessed using 6-methoxy-*N*-ethylquinolinium iodide (MEQ). Working stocks of MEQ were prepared daily over nitrogen as previously described (12). Slices were incubated in 400 μM MEQ for 1 h and then rinsed in MEQ-free ACSF for 10 min before experimentation. Changes in MEQ fluorescence were calibrated using the Stern–Volmer equation as described elsewhere (12). Chloride movement induces cell-volume changes, and therefore cell-volume changes were measured using a calcein fluorescence

assay (13). Calcein-AM was excited at 488 nm and emissions were recorded at 520 nm. Traces were drift-corrected by fitting 1-min stable baseline recordings 5 min before and after treatment onset with a linear regression line. Individual points on the raw trace were then divided by the corresponding points on the regression line (14). Maximum cell-volume changes were determined by perfusing cortical sheets with progressively hypo/hyperosmotic ACSF until the osmolarity change was sufficient to induce >10% cell mortality (assessed by complete loss of calcein fluorescence). Minimum fluorescence was observed at 100 mOsm, whereas maximum fluorescence changes occurred at 500 mOsm. Treatment-induced changes in calcein fluorescence are expressed as the percent change relative to this maximum.

Imaging and Quantification of Cell Death Using Propidium Iodide. Cortical slices were incubated overnight with 6 μg/mL of propidium iodide (PI) at 4 °C to ensure penetration of PI into the tissue. Cortical slices were assigned to one of five groups: (*i*) normoxia (ambient O_2/5% CO_2), (*ii*) 3.5 mM normoxia + iodoacetate + sodium cyanide, (*iii*) anoxia (95% N_2/5% CO_2), (*iv*) anoxia + 25 μM gabazine + 5 μM CGP55845, and (*v*) anoxia + 25 μM gabazine + 5 μM CGP55845 + 50 μM TTX. Each brain slice was placed into a single well in a 12-well tissue plate. Fresh PI (6 μg/mL) was placed into these wells to prevent depletion of the dye. Tissue wells that contained anoxic slices were placed in an enclosed chamber aerated with N_2/CO_2 gas, whereas tissue wells containing cortical slices in the normoxic groups were exposed to room air. Cell death was visualized using a Zeiss Axiovert 200M microscope with a Hamamatsu ORCA-ER camera. Slices were visualized under a 2.5× objective and excited by a mercury lamp at 546 nm and emission at 590 nm controlled by AxioVision (version 4.4; Zeiss) software. Images of cell death were taken at time = 0, 1, 2, and 4 h. To quantify cell death in each slice, slice images were analyzed using ImageJ software (version 1.37; National Institutes of Health). PI fluorescence due to iodoacetate (IAA) treatment was assessed as maximal cell death, and each treatment group was normalized to this maximum.

Pharmacology. Cortical neurons were perfused with pharmacological modifiers as specified in *Results*. Except for dose–response experiments, GABARs were activated by 0.5 or 2.0 mM GABA, which is high relative to turtle $GABA_AR$ binding affinity (15); however, GABA uptake mechanisms in the intact tissue likely reduce the concentration of GABA that actually interacts with receptors (16). Furthermore, stimulus-evoked GABAergic inhibitory postsynaptic potentials in gramicidin-patched cortical neurons could not be completely abolished at [GABA] <1 mM. Therefore, high levels of GABA in the experimental ACSF are required to significantly elevate [GABA] at the synaptic level in deep neuronal tissue. $GABA_A$ and $GABA_B$ receptors were blocked by gabazine (SR-95531; 25 μM) and CGP55845 (5 μM), respectively. Voltage-gated sodium channels were blocked with TTX (2–5 μM). Ischemia was mimicked pharmacologically by perfusion of 3.5 mM iodoacetate and 100 μM sodium cyanide (NaCN). All chemicals were obtained from Sigma Chemical, except CGP55845, which was obtained from Tocris Cookson.

Statistical Analysis. Normalized data were analyzed using two-way ANOVA with a Student–Newman–Keuls post hoc test to compare within and against treatment and normoxic values. Significance was determined at $P < 0.05$, and all data are expressed as mean ± SEM.

1. Shin DS, Buck LT (2003) Effect of anoxia and pharmacological anoxia on whole-cell NMDA receptor currents in cortical neurons from the western painted turtle. *Physiol Biochem Zool* 76:41–51.
2. Pamenter ME, Buck LT (2008) Neuronal membrane potential is mildly depolarized in the anoxic turtle cortex. *Comp Biochem Physiol A Mol Integr Physiol* 150:410–414.
3. Blanton MG, Lo Turco JJ, Kriegstein AR (1989) Whole cell recording from neurons in slices of reptilian and mammalian cerebral cortex. *J Neurosci Methods* 30:203–210.
4. Zhang L, Krnjević K (1993) Whole-cell recording of anoxic effects on hippocampal neurons in slices. *J Neurophysiol* 69:118–127.
5. Ghai HS, Buck LT (1999) Acute reduction in whole cell conductance in anoxic turtle brain. *Am J Physiol* 277:R887–R893.
6. Hewitt SA, Wamsteeker JI, Kurz EU, Bains JS (2009) Altered chloride homeostasis removes synaptic inhibitory constraint of the stress axis. *Nat Neurosci* 12:438–443.
7. DeFazio RA, Keros S, Quick MW, Hablitz JJ (2000) Potassium-coupled chloride cotransport controls intracellular chloride in rat neocortical pyramidal neurons. *J Neurosci* 20:8069–8076.
8. Watanabe M, Wake H, Moorhouse AJ, Nabekura J (2009) Clustering of neuronal K^+-Cl^- cotransporters in lipid rafts by tyrosine phosphorylation. *J Biol Chem* 284: 27980–27988.
9. Pérez-Pinzón MA, Chan CY, Rosenthal M, Sick TJ (1992) Membrane and synaptic activity during anoxia in the isolated turtle cerebellum. *Am J Physiol* 263: R1057–R1063.
10. Pamenter ME, Buck LT (2008) δ-Opioid receptor antagonism induces NMDA receptor-dependent excitotoxicity in anoxic turtle cortex. *J Exp Biol* 211:3512–3517.
11. Buck LT, Bickler PE (1995) Role of adenosine in NMDA receptor modulation in the cerebral cortex of an anoxia-tolerant turtle (*Chrysemys picta belli*). *J Exp Biol* 198: 1621–1628.
12. Inglefield JR, Schwartz-Bloom RD (1999) Fluorescence imaging of changes in intracellular chloride in living brain slices. *Methods* 18:197–203.
13. Hamann S, et al. (2002) Measurement of cell volume changes by fluorescence self-quenching. *J Fluoresc* 12:139–145.
14. Crowe WE, Altamirano J, Huerto L, Alvarez-Leefmans FJ (1995) Volume changes in single N1E-115 neuroblastoma cells measured with a fluorescent probe. *Neuroscience* 69:283–296.
15. Lutz PL, Leone-Kabler SL (1995) Upregulation of the $GABA_A$/benzodiazepine receptor during anoxia in the freshwater turtle brain. *Am J Physiol* 268:R1332–R1335.
16. Frahm C, Engel D, Draguhn A (2001) Efficacy of background GABA uptake in rat hippocampal slices. *Neuroreport* 12:1593–1596.

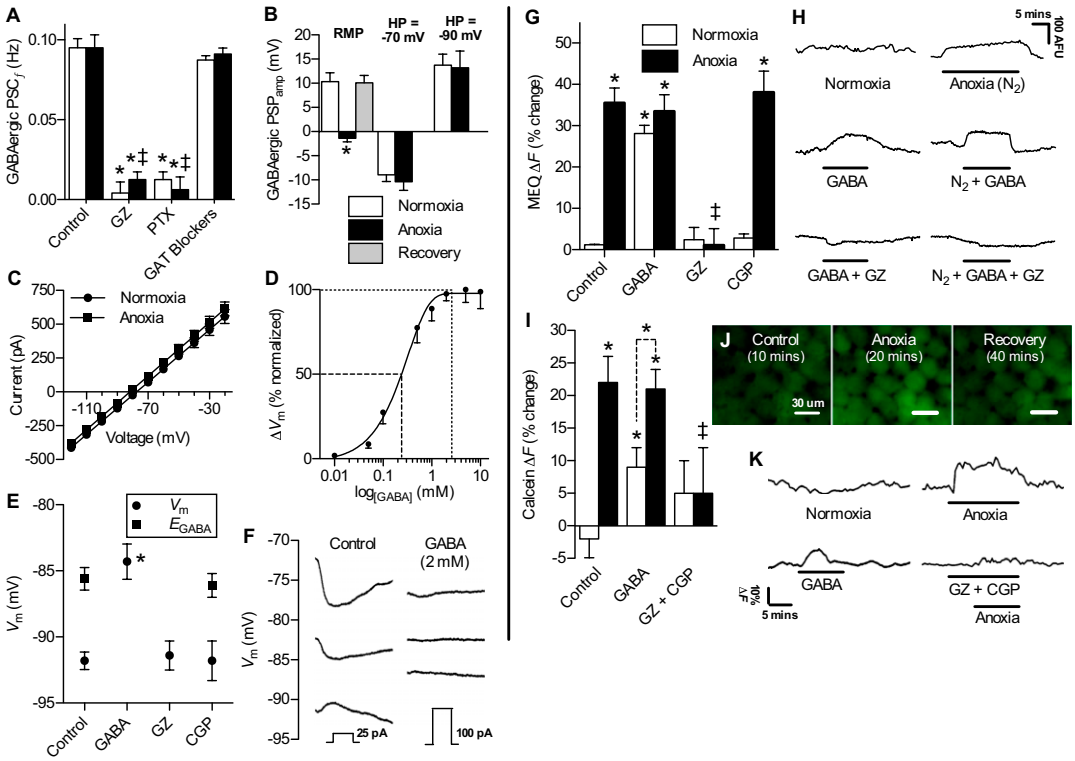

Fig. S1. Slow phasic synaptic GABA$_A$R activity is up-regulated by anoxia and depolarizes membrane potential (V_m) to E_{GABA} accompanied by Cl^- efflux. (*A*) Summary of GABAergic PSC frequency from the neurons in Fig. 2 *B* and *C*. (*B*) Summary of PSP amplitudes at resting membrane potential (RMP), and when neurons were clamped at de- or hyperpolarizing voltage steps from Fig. 2*D* [holding potential (HP)]. To isolate GABAergic PSCs and PSPs in these experiments, neurons were perfused with APV and CNQX (25 μM each). (*C*) Sample *I–V* relationship of pure GABA currents from Fig. 2*E*; E_{GABA} is the *x* intercept. "Pure" GABA currents were determined by subtracting normoxic *I–V* curves from normoxic + GABA *I–V* curves. (*D*) Dose–response relationship of [GABA] versus ΔV_m. (*E*) Summary of normoxic V_m and stimulus-evoked E_{GABA} measured in the perforated-patch configuration. The AMPAR antagonist CNQX was included in the pipette solution to prevent APs. (*F*) Stimulus-evoked PSPs were abolished by 2 mM GABA perfusion. Traces are from consecutive current injections. (*G*) Summary of MEQ fluorescence. (Note: Increased MEQ fluorescence corresponds to reduced $[Cl^-]_c$.) (*H*) Sample MEQ fluorescence recordings from *G*. (*I*) Summary of calcein fluorescence. (Note: Increases in calcein fluorescence correspond to decreased cell volume.) (*J*) Sample calcein fluorescence images of a population of neurons undergoing an anoxic transition with recovery. (*K*) Sample calcein fluorescence recordings from *I*. Raw MEQ and calcein sample traces are averages of 50 neurons from each cortical sheet. Fluorescence changes were assessed after the fluorescent signal stabilized for at least 5 min following treatment onset, and are expressed relative to baseline fluorescence before treatment onset. Black bars represent duration of treatment. Treatments were as in Figs. 1 and 2. Data are mean ± SEM from 4–12 separate experiments. Asterisks indicate significant difference from normoxic controls. Double daggers indicate significant difference from anoxic controls.

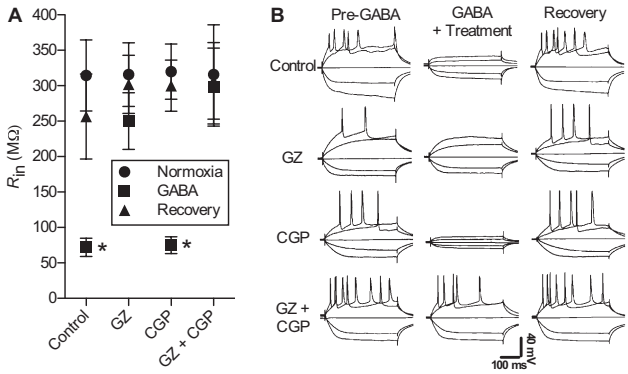

Fig. S2. GABA decreases R_{in} in a GABA$_A$R-sensitive manner. (*A*) Summary of normoxic stimulus-evoked R_{in} measured in the perforated-patch configuration, with CNQX in the pipette solution to prevent APs. (*B*) Sample traces of stimulus-evoked currents. Treatments were as in Figs. 1 and 2; [GABA] = 2 mM. Data are mean ± SEM from 6–12 separate experiments. Asterisks indicate significant difference from normoxic controls. Double daggers indicate significant difference from anoxic controls.

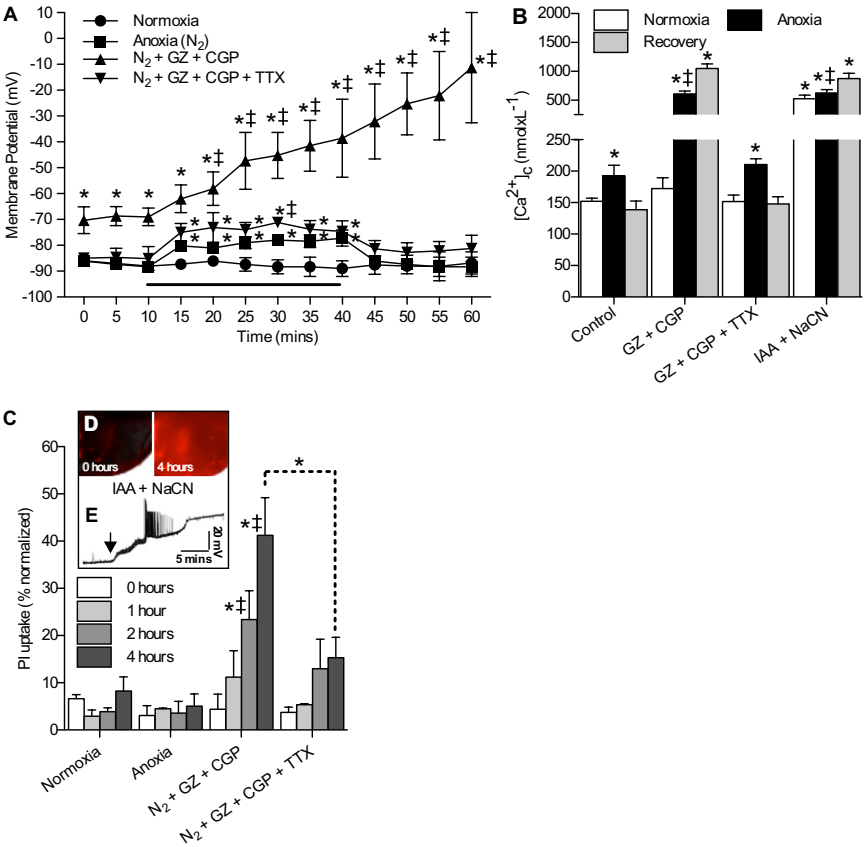

Fig. S3. GABAergic inhibition during anoxia is excitotoxic to turtle neurons. (*A*) Summary of the effects of $GABA_{A+B}R$ antagonists on V_m during a 60-min normoxic-to-anoxic transition with recovery (bar is anoxic period). (*B*) Summary of $[Ca^{2+}]_c$ from cortical sheets treated per *A*. For each experiment, 50 neurons were chosen at random, and the average change of fluorescence in the cell body of these neurons was used for statistical comparison. (*C*) Summary of PI uptake. (*D*) Paired sample PI fluorescence images from a cortical sheet treated with IAA + NaCN (maximum PI fluorescence) at 0 and 4 h. (*E*) Sample V_m recording from a cell treated acutely with IAA + NaCN (arrow indicates treatment onset). Treatments were as in Figs. 1 and 2. Data are mean ± SEM from 9–12 (electrophysiology) or 3–8 (fluorescence) separate experiments. Asterisks indicate significant difference from normoxic controls. Double daggers indicate significant difference from anoxic controls ($P < 0.05$).